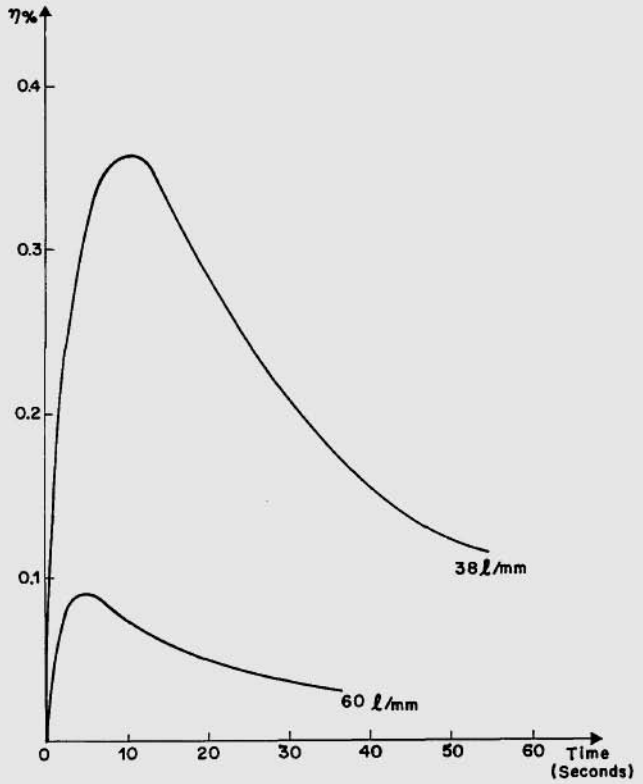

Fig. 4. Behavior of diffraction efficiency as a function of exposure time. The parameter is the spatial frequency of the recorded interference pattern.

was measured, and results are given in Fig. 1, which refers to layers 30, 60, and 90 μm thick. The effect of doubling the dichromate concentration is shown in Fig. 2.

As the DCS plates mentioned above darkened when light fell onto them, their response to interference patterns with different spatial frequencies was studied. The thickness of the layers in this study was 30 μm, dichromate concentration was 32 g, and sugar concentration was 100 g. Diffraction efficiency measurements were made for gratings recorded using the arrangement shown in Fig. 3 in which the 488-nm beams are used to record the interference grating and the 633-nm beam is used to probe the grating. The results are shown in Fig. 4. The efficiency is seen to rise rapidly to its peak value and then fall comparatively slowly. Disappearance of the diffraction spots is much more rapid (a few seconds) when the writing beams are switched off indicating that the gratings are transient in nature. Diffraction efficiency was also measured at a spatial frequency of 100 lines/mm, and a maximum value of 0.0014% was obtained.

From these results we can infer that a phase grating is formed during the first part of the exposure. During this time if an amplitude grating is formed its amplitude modulation should be very small; because transmission is high it cannot be expected to contribute significantly to diffraction efficiency. As the exposure proceeds, transmission of the plate diminishes due to photodarkening and obscures the diffracted light.

Vincent Toal was on leave from the Dublin Institute of Technology, Ireland, when this work was done. He acknowledges the Institute's permission to publish this work. We also acknowledge the financial support of the National Council of Science and Technology, Mexico, and the Center for Investigations in Optics, Mexico.

References

1. J. P. Huignard and J. P. Herriau, "Real-Time Coherent Object Edge Reconstruction with $Bi_{12}SiO_{20}$ Crystals," Appl. Opt. **17**, 2671–2672 (1978).
2. S. Calixto and R. A. Lessard, "Holographic Recording and Reconstruction of Polarized Light with Dyed Plastic," Appl. Opt. **23**, 4313–4318 (1984).
3. S. Calixto and R. A. Lessard, "Real-Time Holography with Undeveloped Dichromated Gelatin Films," Appl. Opt. **23**, 1989–1994 (1984).
4. H. M. Smith, *Holographic Recording Materials* (Springer-Verlag, Berlin, 1977).
5. B. J. Chang and C. D. Leonard, "Dichromated Gelatin for the Fabrication of Holographic Optical Elements," Appl. Opt. **18**, 2407–2417 (1979).
6. S. Calixto, "Dry Polymer for Holographic Recording," Appl. Opt. **26**, 3904–3910 (1987).
7. C. Solano, R. A. Lessard, and P. C. Roberge, "Methylene Blue Sensitized Gelatin as a Photosensitive Medium for Conventional and Polarizing Holography," Appl. Opt. **26**, 1989–1997 (1987).
8. White sugar was obtained at the supermarket.
9. D. Meyerhofer, "Spatial Resolution of Relief Holograms in Dichromated Gelatin," Appl. Opt. **10**, 416–421 (1971).

Experimental considerations for 2-D acoustooptic spectrum analysis

Homayoon Ansari, Brian D. Metscher, and James R. Lesh

The authors are with Jet Propulsion Laboratory, 4800 Oak Grove Drive, Pasadena, California 91109.
Received 26 March 1990.
0003-6935/90/365317-03$02.00/0.

A 2-D acoustooptic spectrum analyzer with the associated reference function generator and real-time image processor has been constructed. The operation of the analyzer and the experimental considerations for obtaining a high resolution spectrum in real time are described. Key words: *Spectrum analysis, acoustooptic, Bragg cells.*

Two-dimensional acoustooptic spectrum analysis (2-D AOSA)[1,2] can potentially be utilized in applications involving a search for rf signals or rf interference characterization, both of which require high resolution and a wide analysis bandwidth. We have constructed a 2-D AOSA based on the discrete Fourier transform architecture demonstrated in Ref. 2. The resolution, bandwidth, and analysis time of the 2-D AOSA depend on the characteristics of its electronic as well as optical components. In this Letter we describe the operation of the 2-D AOSA and the experimental considerations for obtaining a high resolution 2-D spectrum in real time.

The optical setup for the 2-D AOSA is shown in Fig. 1, which consists of a laser, a pair of orthogonally oriented

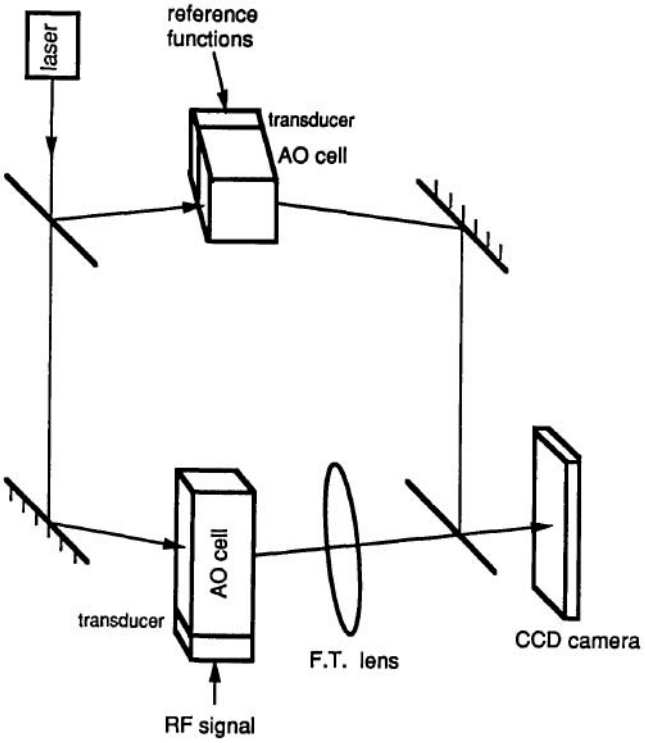

Fig. 1. Two-dimensional AOSA architecture.

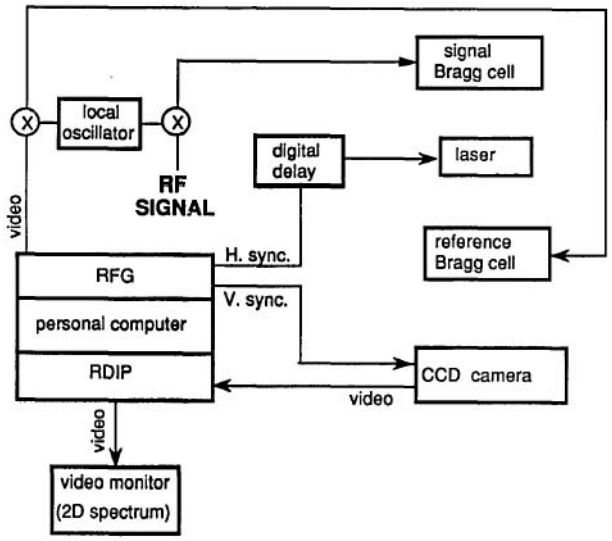

Fig. 2. Electronic layout of 2-D AOSA.

Bragg cells, and a CCD camera. The lower arm of the interferometer in Fig. 1 receives the signal and performs space integration, whereas the upper arm receives a sequence of inphase reference function lines in the form of a sampled distributed local oscillator (DLO), which is used to perform time integration. The signal from the lower Bragg cell is first focused by the Fourier transforming lens along the direction of the signal Bragg cell, and a 1-D coarse resolution spectrum is thus obtained on the CCD array. The focused signal is then mixed wih the reference DLO and time integrated on the CCD array. Form this a fine resolution spectrum is obtained along the direction of the reference Bragg cell in each coarse resolution bin, resulting in a 2-D spectrum. An unwanted signal dependent bias term is also created, but this term can be subtracted out electronically after detection.

The electronic layout of the 2-D AOSA is shown in Fig. 2, which includes a personal computer containing a high speed digital graphics board used as a reference function generator (RFG) and a real-time digital image processor (RDIP) used to grab the CCD frames and perform spectral bias removal. The resolution and bandwidth of the analyzer depend on the number of pixels in the CCD array and the time–bandwidth products of the two Bragg cells. However, the resolution and bandwidth also depend on the characteristics of the RFG. Furthermore, the analysis time depends on the CCD integration time as well as on the characteristics of the RDIP. The characteristics of the RFG and RDIP are discussed.

The frequency range of the reference DLO described earlier must be matched to the coarse resolution of the analyzer to avoid aliasing or blind regions in the 2-D spectrum. Since the coarse resolution is limited by the inverse time aperture of the signal Bragg cell to ~30 kHz in our case, the RFG must be able to generate a DLO with at least this frequency range to analyze the whole length of each coarse resolution bin with fine resolution. The RFG in Fig. 2 contains a video buffer memory with 2 milion 8-bit pixels storing the sequence of reference function lines and read out at 100 Mpixels/s. The RFG output consists of an NTSC format video signal with the standard line and frame trigger signals. Before entering the reference Bragg cell, this video signal is put on a 75-MHz carrier, which matches the center frequency of the reference Bragg cell. Figure 3 shows an oscilloscope trace of the first few lines of the programmed RFG output forming the 30-kHz DLO discussed above. The digital delay pulse generator in Fig. 2 provides a precise jitter-free delay between the line trigger signal and the laser pulses so that the reference function lines and laser pulses coincide in the reference Bragg cell with no temporal fluctuatin, which may smear the time integrated distribution on the CCD array. The frame trigger signal from the RFG is used to trigger the CCD camera. The digital storage and generation of the reference function lines allows the capability of matching the size of each fine resolution bin to the size of the CCD pixels.

The RDIP in Fig. 2 grabs and stores spectral and bias frames and performs bias subtraction, resulting in a bias-free spectrum on the output video monitor. It contains four 512- × 512- × 8-bit video frame buffers and has a frame grabbing rate of 30 frames/s, which matches the frame rate of the CCD array. Low level programming of the RDIP allows interimage operations to update the bias in real time before elimi-

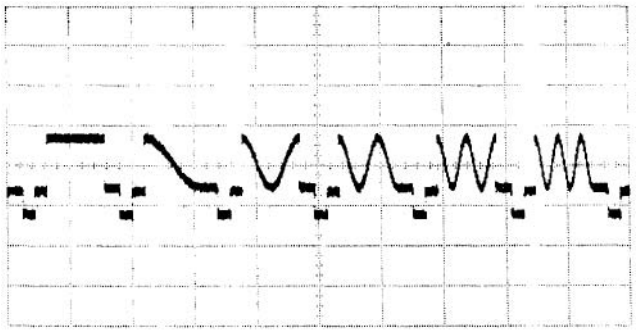

Fig. 3. First six lines of digitally generated reference function. Horizontal scale: 10 μs/div.

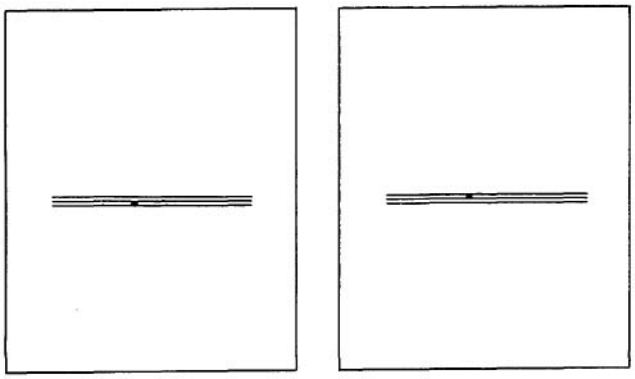

Fig. 4. Monitor displays for two single-tone signals after bias subtraction. Coarse and fine frequencies are along the horizontal and vertical directions, respectively. The left and right displays correspond to input signal frequencies of 10.022415 and 10.022716 MHz, respectively. Horizontal grid lines are superimposed on the CCD output.

nating it. In one mode of operation, an incoming CCD frame is grabbed and stored in one of the frame buffers designated as the bias frame buffer. All subsequent CCD incoming frames are then subtracted from this bias frame, stored in a second frame buffer designated as the spectral frame buffer, and displayed on the monitor as the bias-free spectrum. The spectral frame rate in this mode of operation is equal to the CCD frame rate of 30 frames/s. However, this mode of operation does not allow for the change in bias from frame to frame. In another mode of operation, the bias frame is updated after each frame subtraction, resulting in a spectral frame rate of 15 frames/s. A spectral frame rate of 30 frames/s can also be obtained in this mode of operation by using two bias frame buffers $B1$ and $B2$, updating the incoming CCD frame alternately in one of the bias frame buffers (e.g., $B1$) while simultaneously subtracting the incoming frame from the other bias frame buffer $B2$ and storing the difference frame in the spectral frame buffer.

With the RDIP, it is also possible to perform further postdigital processing to enhance the output spectrum. One example is contrast enhancement and edge detection to identify weak narrowband signals. Another more significant example is processing over a sequence of CCD frames to obtain superfine[2] subhertz resolution.[3,4]

Figure 4 shows the monitor displays after bias subtraction for two single tone signals separated by 301 Hz. The spots on the monitor are space and time integrated peaks with the fine frequency along the vertical direction. The spots are separated by their full width, indicating that a fine resolution of ~150 Hz has been achieved. The horizontal lines are overlay grid lines superimposed on the CCD output for display purposes. The number of fine frequency channels of the system obtained in this manner is ~100,000.

In this paper, the optical and electronic setups for a 2D AOSA were described, and the reference function generator and real-time image processor were shown to be critical components for obtaining a high resolution spectrum in real time.

This work was carried out by the Jet Propulsion Laboratory, California Institute of Technology, under contract with the National Aeronautics and Space Administration.

References

1. T. R. Bader, "Acoustooptic spectrum analysis: a high performance hybrid technique," Appl. Opt. **18**, 1668–1672 (1979).
2. K. Wagner and D. Psaltis, "Time and Space Integrating Acousto-Optic Folded Spectrum Processing for SETI," Proc. Soc. Photo-Opt. Instrum. Eng. **564**, 209–223 (1985).
3. H. Ansari, B. Metscher, and J. Lesh, "Three-Dimensional Acousto-Optic Spectrum Analysis," To be published in Opt. Lett. **XX**, 000–000 (1990).
4. H. Ansari and J. Lesh, "Superfine Resolution Acousto-Optic Spectrum Analysis," submitted to Applied Optics.